Geophysical Research Letters

RESEARCH LETTER
10.1029/2025GL117684

Whitecaps, Bubbles and Advection: Insights From Concurrent Measurements in the Open Ocean

Maria Bjørnestad[1], Trygve Halsne[1], Mika Malila[1], Alvise Benetazzo[2], Filippo Bergamasco[3], Mara Pistellato[2,3], Adrian H. Callaghan[4], Silvio Davison[2], Joe Peach[4], Göran Broström[1,5], and Øyvind Breivik[1,6]

[1]Norwegian Meteorological Institute, Bergen, Norway, [2]Istituto di Scienze Marine, Consiglio Nazionale delle Ricerche, Venice, Italy, [3]Department of Environmental Sciences Informatics and Statistics, Università Ca' Foscari, Venice, Italy, [4]Department of Civil and Environmental Engineering, Imperial College London, South Kensington, UK, [5]Department of Earth Science, University of Gothenburg, Gothenburg, Sweden, [6]Geophysical Institute, University of Bergen, Bergen, Norway

Abstract Field measurements of breaking waves and bubble depths were obtained using a stereo video system collocated with a submerged acoustic Doppler current profiler (ADCP) in the central North Sea. We discriminate between two bubble depths that define an active near-surface layer and a deeper layer. The active layer intermittently sees short-lived injected bubble depths from breakers whereas the deeper layer is dominated by persistent passive bubble plumes that remain visible for more than 50 mean wave periods. We augment traditional single-beam bubble detection methods by utilizing all five beams of the ADCP to achieve broader spatial coverage of bubble plume measurements. The combined wave and bubble observations reveal that deep bubble plumes often occur offset spatially from surface whitecaps, suggesting that Langmuir-type circulation plays a role in the formation and persistence of deep bubble plumes through vertical and horizontal advection.

Plain Language Summary Bubbles created by breaking waves are important for the exchange of gases between the atmosphere and ocean. Using a submerged echosounder and a pair of video cameras on a nearby platform, we simultaneously measured breaking waves from above and air bubbles from below the sea surface in open-ocean conditions in the North Sea. When waves break, a near-surface layer of relatively large bubbles is created for a short amount of time, and a clear relation with surface foam from the breaking waves is observed. Smaller bubbles can be influenced by currents and turbulence, and be transported both vertically and horizontally. These deeper bubble clouds last much longer and their behavior is not directly connected to surface wave breaking events.

Maria Bjørnestad and Trygve Halsne contributed equally to this work.

Key Points:

- We present collocated stereo video and ADCP data of breaking waves and bubble depths in open-ocean conditions
- Short-lived bubble injection depths depend locally on wave breaking; deep plumes remain longer and are disconnected from wave breaking
- ADCP's multibeam geometry reveals advection of bubble plumes in vertical and horizontal directions

Supporting Information:

Supporting Information may be found in the online version of this article.

Correspondence to:

T. Halsne,
trygve.halsne@met.no

Citation:

Bjørnestad, M., Halsne, T., Malila, M., Benetazzo, A., Bergamasco, F., Pistellato, M., et al. (2025). Whitecaps, bubbles and advection: Insights from concurrent measurements in the open ocean. *Geophysical Research Letters*, *52*, e2025GL117684. https://doi.org/10.1029/2025GL117684

Received 30 JUN 2025
Accepted 20 OCT 2025
Corrected 18 NOV 2025

This article was corrected on 18 NOV 2025. See the end of the full text for details.

Author Contributions:

Conceptualization: Maria Bjørnestad, Trygve Halsne, Mika Malila, Alvise Benetazzo
Formal analysis: Maria Bjørnestad, Trygve Halsne, Mika Malila
Funding acquisition: Øyvind Breivik
Investigation: Maria Bjørnestad, Trygve Halsne, Mika Malila

1. Introduction

Breaking waves create patches of foam, or whitecaps, on the surface and inject air bubbles into the water which augments the transfer of gasses across the air-sea interface, and affects the upper-ocean acoustics. Breaking waves also control the interfacial fluxes of energy and momentum, important for mixed-layer dynamics (Callaghan et al., 2016; Deane & Stokes, 2010; Deike, 2022; D. Farmer et al., 1993). Whitecaps are the main source of bubbles in the upper ocean, but it is hard to establish an unambiguous relation between the breaking waves and the depth that the bubbles reach. There are at least two important factors complicating the relation: (a) the presence of small-scale dynamics that transport the smallest bubbles within the sub-surface layer and (b) inexact quantification of bubble depths from established bubble detection methods.

The fluxes of turbulent kinetic energy (TKE) and momentum from wave energy dissipation generate upper-ocean currents and vorticity that may interact with the wave-induced Stokes field and generate Langmuir circulation (e.g., Callaghan et al., 2016; Deike et al., 2017; Leibovich, 1983; Pizzo et al., 2016; Pizzo & Melville, 2013; Strand et al., 2020). For decades, such turbulent flows have been linked to the vertical transport of bubbles (Benetazzo et al., 2024; Liang et al., 2012; Peláez-Zapata et al., 2024; S. Thorpe et al., 2003; Thorpe, 1982, 1984; Woolf, 1997), and it has recently been shown that Langmuir-type currents and enhanced TKE dissipation rates coincide with the deep bubble entrainment depicted by echo sounders (see Figures 11, 12, and 16 in Fisher and Nidzieko (2024), Scully and Zippel (2024), Andriatis et al. (2024), respectively). However, sparse observations and limitations in commonly used measurement techniques have contributed to a lack of consensus on how to

Methodology: Maria Bjørnestad, Trygve Halsne, Mika Malila, Filippo Bergamasco, Mara Pistellato, Adrian H. Callaghan, Silvio Davison, Joe Peach
Project administration: Øyvind Breivik
Resources: Göran Broström
Software: Maria Bjørnestad, Trygve Halsne, Mika Malila, Filippo Bergamasco, Mara Pistellato, Adrian H. Callaghan, Silvio Davison, Joe Peach
Supervision: Øyvind Breivik
Validation: Maria Bjørnestad, Trygve Halsne, Mika Malila
Visualization: Maria Bjørnestad, Trygve Halsne
Writing – original draft: Maria Bjørnestad, Trygve Halsne, Mika Malila
Writing – review & editing: Alvise Benetazzo, Filippo Bergamasco, Mara Pistellato, Adrian H. Callaghan, Silvio Davison, Göran Broström, Øyvind Breivik

parameterize such advective effects into empirical relationships between observed bubble depths and integrated sea parameters.

Active vertically oriented sonar systems, that is, echo sounder measurements that resonate with bubble radii $\ll$ 1 mm, estimate bubble penetration depths (Vagle & Farmer, 1992; Vagle et al., 2010; Thorpe, 1982). However, in contrast to passive acoustic and optical methods, they do not give quantitative estimates of the bubble size distribution, which is important for the dynamics in the upper few meters (e.g., Czerski et al., 2022; D. M. Farmer et al., 1998; Vagle & Farmer, 1998). Owing to the simplicity and robustness of these devices, echo sounders are the most frequently used platform for field measurements of bubble depths; they have primarily been used for observing large, slowly fluctuating bubble plumes that reach depths much larger than the significant wave height H_s (e.g., Benetazzo et al., 2024; Strand et al., 2020; Thorpe, 1982). Observed bubble plume depths have recently also been linked in a statistical sense to the sea-surface whitecapping activity in the vicinity of the bubble observations (e.g., Cifuentes-Lorenzen et al., 2023; Derakhti et al., 2024; Peláez-Zapata et al., 2024). Above-water measurements of whitecap foam evolution can be used to infer the initial short-duration injection of bubbles during active wave breaking (Callaghan et al., 2016, 2017), but the link between co-located surface whitecaps and bubble depths is hitherto unknown.

Here, we analyze sonar measurements of bubble injection and penetration depths estimated using two empirical bubble detection methods, as defined by Derakhti et al. (2024), and study their behavior relative to surface whitecaps with a stereo video system. In Section 2, we give a brief description of the methods, with more comprehensive descriptions provided in Supporting Information S1 (hereafter SI). An isolated whitecap event is analyzed in Section 3, and the dynamical relationship between whitecaps and bubble depths over many wave periods is elaborated in Section 4. The behavior of deeper plumes is described in Section 5.

2. The Ekofisk Experiment: Data and Methods

A stereo video system reconstructs the three-dimensional sea surface wave field. Such a system has been operated since 2017 north of the Ekofisk 2/4 K offshore platform in the central North Sea. During fall 2022, a five-beam Nortek Signature 500 kHz ADCP was deployed within the field of view of the stereo cameras (Figure 1a). We obtained a total of six 20 min concurrent segments of sea surface elevation, surface whitecaps, mean currents and bubble depths. These segments were recorded on 3 days with different sea states. Three segments have been examined here: two segments on 16-09-2022 (T16 and T17, datetime values are in UTC) which exhibited extensive wave breaking, with mean 10 m wind speed $U_{10} = 15\ \mathrm{m\,s^{-1}}$ and significant wave height $H_s = 6$ m. The third segment on 11-03-2022 T13 had limited wave breaking in relatively calm conditions, with $U_{10} = 2\ \mathrm{m\,s^{-1}}$ and $H_s = 2.6$ m. See Table 1 and Supporting Information S1 for more details about the acquisition setup and met-ocean conditions.

Every 20-min segment of images acquired at 5 Hz was processed using the Waves Acquisition Stereo System (WASS) software (Benetazzo et al., 2012; Bergamasco et al., 2017; Pistellato et al., 2021). We identified and tracked individual whitecaps with the Automated Whitecap Detection And Tracking (AWDAT) method (Peach et al., 2025). The output is shown in Figure 1, and more details about the processing is given in Section S1 of Supporting Information S1.

The ADCP was configured to measure waves and currents with high resolution echogram mode enabled, mounted on a sub-surface buoy at approximately 45 m depth. The vertical echogram from the center beam, B5, yields an acoustic scattering cross section per unit volume at different depths. This backscattering volume increases with distance, and the backscatter intensity must be corrected for signal loss and transmit range when transforming to volumetric backscatter, Sv (Section S2 in Supporting Information S1). A spatio-temporal view of collocated WASS, AWDAT, and Sv output is shown in the Movie S1.

The air-bubble entrainment depth is commonly determined from Sv by setting a threshold (e.g., Benetazzo et al., 2023; Cifuentes-Lorenzen et al., 2023; Derakhti et al., 2024; Peláez-Zapata et al., 2024; Thorpe, 1982; Vagle et al., 2010). Active echogram measurements do not quantify the bubble size distribution. The bubble size is therefore approximated by bubble-resonant frequencies, which to leading order are a function of the depth and transmit frequency (Vagle & Farmer, 1992), here $\sim$10 μm (Section S2 in Supporting Information S1).

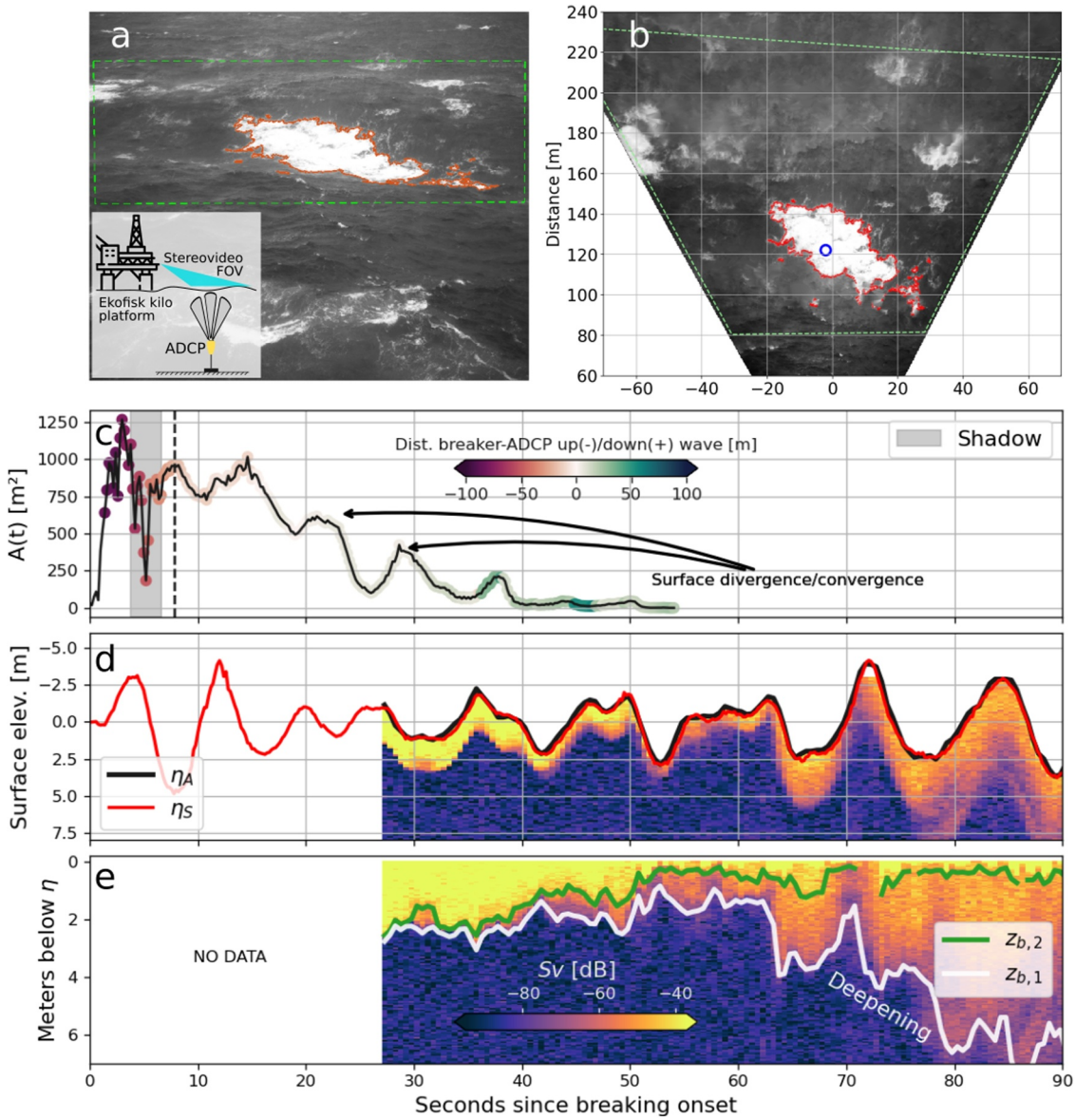

Figure 1. A single breaking event starting at 16-09-2022 T16:59:38.5. Panels (a, b) show the whitecap event at 16:59:46.3 in camera and ortho-rectified view, respectively. The whitecap boundaries are outlined in red, the green dashed lines indicate the whitecap tracking area, and the blue circle in panel (b) shows the surface area ensonified by beam B5. Panel (c) shows the time evolution of the whitecap event area, with colors indicating the Euclidean distance between the whitecap center-point and B5. Negative values are in the up-wave direction (i.e., away from the camera). The vertical dashed line is placed at time 16:59:46.3, and the gray area indicates significant shadowing. Panel (d) shows the collocated sea surface elevation from the stereo video system (η_S) and B5 (η_A), overlaying the volumetric backscatter (Sv) profile from B5. In panels (d, e), the first 27 s are missing, since the ADCP recording started at the top of the hour. Panel (e) shows the Sv profile in surface-following coordinates with bubble depths from $z_{b,1}$ to $z_{b,2}$.

We estimate bubble depths following the two bubble detection methods (BDMs) defined by Derakhti et al. (2024). The first, BDM1, is similar to most other works with a threshold of $Sv_{tr,1} = -70$ dB. The second, BDM2, has $Sv_{tr,2} = Sv_{tr,1} + 25$ dB. Derakhti et al. (2024) argue that such an increase by two orders of magnitude will identify regions of high void fractions as well as scatterers that have much larger volume and size than the resonant bubble size. As noted by Czerski et al. (2022), these thresholds are somewhat arbitrary since the echogram provides no detailed information about the bubble size distribution. Nevertheless, this technique is well established, and as we will see, distinguishes an active near-surface layer from a deeper layer of passive bubbles. The bubble depths from the low-threshold method (BDM1) and the high-threshold method (BDM2) are denoted

Table 1
The Met–Ocean Conditions Including Wave Group and Bubble Plume Parameters for the Measurement Segments in 2022 With Wave Breaking (Denotes Segment Without Stereo Video Coverage)*

Date	H_s	$T_{m_{02}}$	U_{10} (dir)	$\bar{\tau}_g$	$\bar{\tau}_P$ (med)	$\bar{\tau}_{P,dur}$ (med)	$z_{p,\max}$	#Plumes	#Groups
09–16T15*	5.8	7.8	15 (335)	69	79 (67)	30 (21)	13.2	13	18
09–16T16	5.9	7.6	15 (334)	62	63 (44)	25 (18)	14.3	18	19
09–16T17	5.8	7.4	15 (335)	63	54 (59)	24 (20)	15.4	21	19
11-03T13	2.6	6.0	2 (240)	51	91 (105)	9 (4)	3.4	11	24
Units	[m]	[s]	[m/s] (deg)	[s]	[s]	[s]	[m]	–	–

Note. Average 10 m wind speed U_{10} (direction coming from, clockwise from North). Statistical wave group and plume parameters from a threshold-crossing analysis include the mean wave group period $\bar{\tau}_g$, mean wave plume period $\bar{\tau}_P$ (median), mean wave plume duration $\bar{\tau}_{P,dur}$ (median), and the maximum bubble depth $z_{p,\max}$. The number of plumes and groups are denoted by #. For more details see Supporting Information S1.

$z_{b,i} = |\eta_A - z_{c,i}|, i = 1,2$, where subscript "c" denote the depth coordinate, and thus measured relative to the surface elevation η_A as observed by the ADCP.

We collocated the sea surface elevation time series η_S from the stereo system with η_A over each 20-min segment, and got a correlation of 0.99 (Section S6, Figure S2 and Table S2 in Supporting Information S1). A sample from 16-09-2022 T17 is shown in Figure 1d.

3. Single Breaking Waves and Bubble Injection Depths

The experimental setup allows us to track whitecaps and bubble depths from above and below the ocean surface simultaneously. By inspection, it appears that in the most energetic sea state ($H_s > 5$ m), shorter waves break on top of longer waves, in qualitative agreement with the theory of short-wave modulation by long waves (Longuet-Higgins, 1984). Unfortunately, there are very few cases where a large-amplitude long wave, say around the peak frequency, breaks in the vicinity of the ADCP.

A peak-period breaking wave is shown in Figure 1, where the local wave height is almost 10 m and the local wave period is 8 s. The whitecap event is shown in Figures 1a and 1b with its boundaries outlined in red. The breaking event started about 60 m up-wave of B5, and collapsed on top of it (blue circle). The temporal evolution of the whitecap area $A(t)$ followed a characteristic development, increasing rapidly after the onset of breaking (during the active phase) before gradually decreasing after the breaker had passed (Figure 1c). We found occasional shadowing by the tallest wave crests. Fluctuations in $A(t)$ in the decay phase are most likely due to contraction and expansion of the foam patch caused by the orbital velocities, which implies local, transient, convergence and divergence zones in the flow field that may cause small vertical fluctuations in the bubble depths. The time evolution of the crest length shows a similar behavior (Figure S4 in Supporting Information S1). The ADCP started measuring after the wave started breaking, see Figure 1d, but while there was still foam present. The vertical sub-surface column was particularly "clean" during this event, meaning that the backscatter intensity values for both low- and high-threshold methods reflected the same event.

To compare the ADCP bubble depth measurements with bubble injection depths inferred from whitecap coverage, we use the laboratory experiment-based theory of Callaghan et al. (2016), which provides an estimate of the maximum value of the mean bubble injection depth at the time of maximum foam area $\bar{z}_p = 0.11(\pm 0.01)\tau_{\text{decay}}^{0.84(\pm 0.11)}$, where A_0 is the maximum foam area and $\tau_{\text{decay}} = A_0^{-1}\int_{t_{A_0}}^{\infty} A(t)\,dt$ is the integral decay time scale. This gives us an estimated mean injection depth of $\overline{z_p} = 1.5$ m at the time of maximum foam area, which resembles the order of magnitude of the depth of $z_{b,2} \simeq 2$ m (Figure 1e), and supports the general observation from Callaghan et al. (2024) that the injection depth values are relatively shallow. Despite limitations related to the unknown bubble size, the uncertainty of the estimate of A_0 and the effects of surfactant-driven foam stabilization (Callaghan et al., 2017), the similarity between the observed and theoretical bubble injection depths suggests that the high-threshold method is consistent with the parameterizations inferred from laboratory experiments of breaking waves (Callaghan et al., 2016).

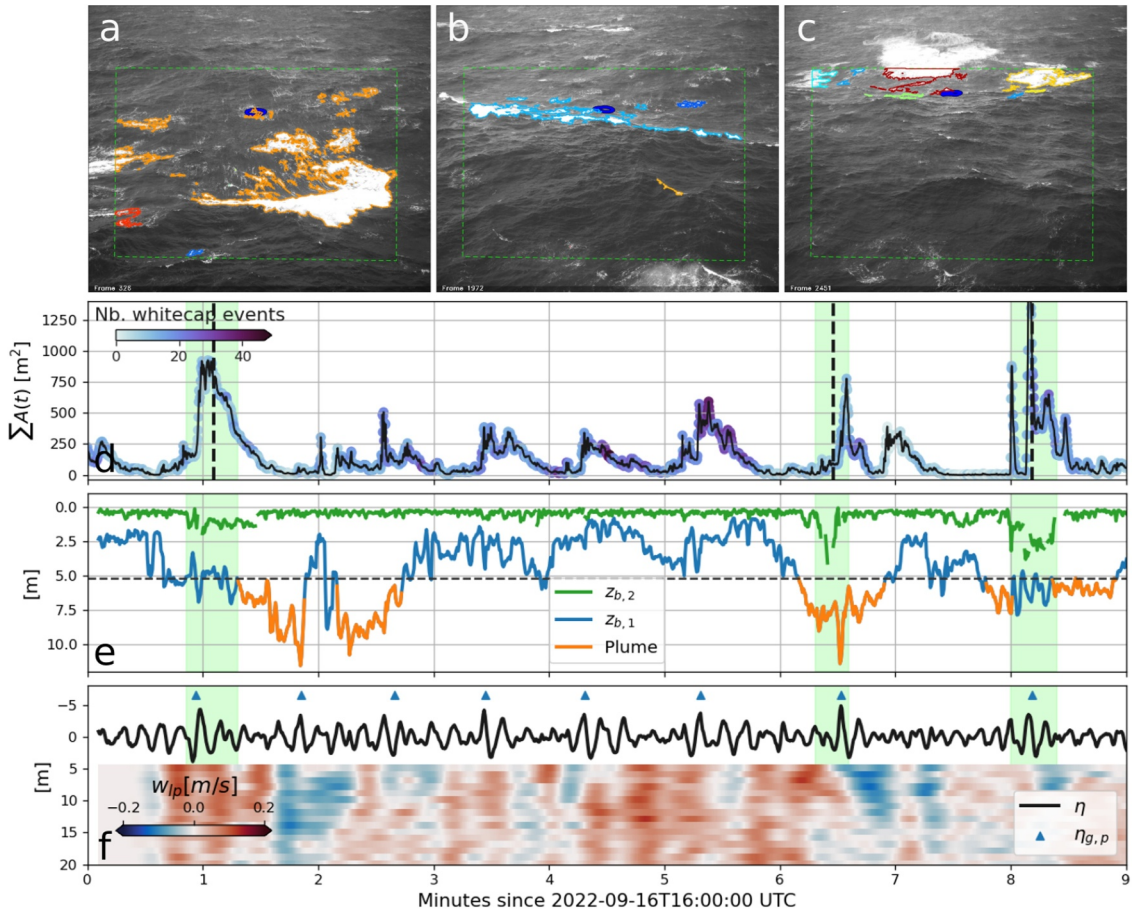

Figure 2. Temporal evolution in whitecap events. Upper row show snapshots of the sea surface with segmented breaking events from AWDAT (a–c), where different colors indicate specific events; panel (d) shows the sum of whitecap area in each frame (colored by the number of detected breaking events); panel (e) shows the temporal evolution in bubble depths from $z_{b,1}$ (blue/orange) and $z_{b,2}$ (green). Orange colored $z_{b,1}$ values indicate the occurrence of bubble plumes according to our definition, and dashed horizontal line denote the mean penetration depth $\bar{z}_{b,1}$; panel (f) shows the vertical distribution of low-pass filtered vertical velocities from beam B5, together with η_A. Blue triangles indicate the peak of the wave groups. For panels (d, e), green shaded background areas indicate times when waves are actively breaking in the vicinity of beam B5, and vertical dashed lines denote the time of panels (a–c), from left to right, respectively.

During the remainder of the time series in Figure 1, there were no significant whitecap events. Interestingly, the two bubble depth estimates diverge; the injected bubble depth ($z_{b,2}$, high-threshold method) stays, as expected, close to the sea surface while the lower layer ($z_{b,1}$, low-threshold method) penetrates deeper down into the water column and reaches depths up to 10 m (not shown). In the subsequent sections, we will investigate in more detail the different, and apparently disconnected, dynamic response of these two bubble depths, and show how they represent local (active near-surface layer) and non-local (deeper layer) processes with respect to the intermittent surface breakers.

4. Whitecaps and Deep Bubble Plumes

A 9 min time series of the surface whitecaps and bubble depths is shown in Figure 2. We find an increase in the sum of whitecap area ($\sum A(t)$, panel d), which most of the time coincides with the peak of the wave groups (triangles in panel f); this agrees with the findings by Malila et al. (2022). We find $z_{b,2}$ to increase when larger waves break in the vicinity of the ADCP. Such events are indicated by the three green-colored time-intervals in panels d–f, which correspond to the camera snapshots in panels a–c, respectively. These bubbles reach depths of approximately 3 m. As expected, $z_{b,1}$ represents larger depths than $z_{b,2}$. Figure 2e showcases depths exceeding 10 m, while 15 m was reached 10 min later (Table 1). Apparently, there is no clear connection between the temporal modulation of $z_{b,1}$ and $\sum A(t)$.

To characterize bubble *plumes*, that is, deeper vertical $z_{b,1}$-structures larger than H_s, we use a similar approach as for wave groups, see Section S5 in Supporting Information S1. The occurrence of plumes is highlighted in Figure 2e. At times, plumes occur after a series of breaking events (see around 1 min in panels d–e). However, this is not always the case. Most of the time, plumes appear temporally offset from the surface breaking activity (e.g., between 2–3 and 7–8 min). As such, their dynamic response is disconnected from the actively injected bubble depths near the surface.

Due to a lack of near-surface wind measurements, the turbulent Langmuir number $\mathrm{La}_t = \sqrt{u^*/u_{S(z=0)}}$ was estimated using friction velocity u^* and surface Stokes drift $u_S(z = 0)$ from a wave hindcast archive (Breivik et al., 2022; Haakenstad et al., 2021). The value of La_t was approximately 0.3 during the periods analyzed here, suggesting that the sea state was conducive to Langmuir-type instability (McWilliams et al., 1997). In the presence of such small-scale wave-induced currents, it is expected that the small bubbles, with radii $\mathcal{O}(10^1)$ μm, will be both vertically and horizontally advected (S. Thorpe et al., 2003). According to Thorpe (1982), the rise velocity of such small bubbles is $\mathcal{O}(10^0)$ cm/s in quiescent water, and likely smaller in turbulent conditions. Hence, small bubbles rise $\mathcal{O}(10^0)$ m in a minute, which is small compared with the length scales shown in Figure 2e.

We find that the low-pass filtered vertical velocities w_{lp} ($f < 1/20$ Hz) from B5, that is, possibly currents of Langmuir-type, only occasionally coincide with the evolution of deeper plumes (Figures 2e and 2f). In fact, we often find that the plumes deepen despite w_{lp} being positive. As shown in the following section, this offset in plume depths and vertical velocities is likely a feature of non-local bubble plumes being horizontally advected in the water column.

5. Spatio-Temporal Offset Between Surface Whitecaps and Bubble Plumes

To increase the spatial coverage of the bubble plumes, we make use of the full five-beam configuration of the ADCP. As such, two relevant backscatter intensities are considered; the first is the high-resolution echogram mode, which is the most common backscatter intensity profile used for bubble depth retrievals (Benetazzo et al., 2023; Derakhti et al., 2024); the second utilizes the burst-mode backscatter intensity measurements along the slanted beams B1–B4, which is used for computing currents. However, the burst-mode profiles are acquired using a different configuration than the echogram mode, which includes differences in signal resolution, range resolution, and transmit pulse duration. As a result, the backscatter intensity distributions from the echogram- and burst-mode measurements are different. More detailed information on the full five-beam bubble depth retrieval method is given in Section S3 of Supporting Information S1.

The spatio-temporal offset between surface whitecaps and bubble plumes is highlighted in Figure 3. Cases 1 and 2, taken from 03-11-2022 T13 to 16-09-2022 T16, represent relatively calm and energetic sea states, respectively (Table 1). The largest breaker encountered in Case 1 is shown in Figures 3b and 3c. A plume was detected by beam B2 (while the ADCP was rotating clockwise) about 2 minutes after breaking, see panel e. After almost 5 minutes (about $50\,T_{m_{02}}$), the plume was detected by B5, see panel d. At this stage, the plume had become shallower, but retained its shape and extent.

The initial breaking crest propagated in the mean wind direction (panel b, not shown). Despite limited knowledge of the rate of horizontal expansion of such plumes, we would expect the plume direction to be aligned with the wave momentum—at least in the early stages of breaking. The current at the closest point in space and time (vertical distance 38.5 m from the ADCP) was westward (Figure 3a). The advection of the plume from B2 to B5 took around 3 min. This aligns with the background mean current of 0.09 m s^{-1} and the beam separation distance of about 20 m, which gives 220 s (see Figure S5 in Supporting Information S1 for vertical time-averaged current profiles). The hypothesized plume trajectory is shown in Figure 3b. This interpretation is supported by the fact that there were no large whitecaps within the domain between the first breaker and the plume arrival time at B5. The only exception was a smaller wave that broke 32 m away after the bubble plume had arrived at B5, as indicated in Figure 3c. In summary, Case 1 suggests that deeper bubble plumes are long-lived and may be advected considerable distances by the ambient currents.

We also observe advection of bubble plumes occurring during more energetic conditions. In Case 2, a deep plume was advected from right to left (Figure 3 right panels); the plume was first observed in S4, advected to S1. Due to

10.1029/2025GL117684

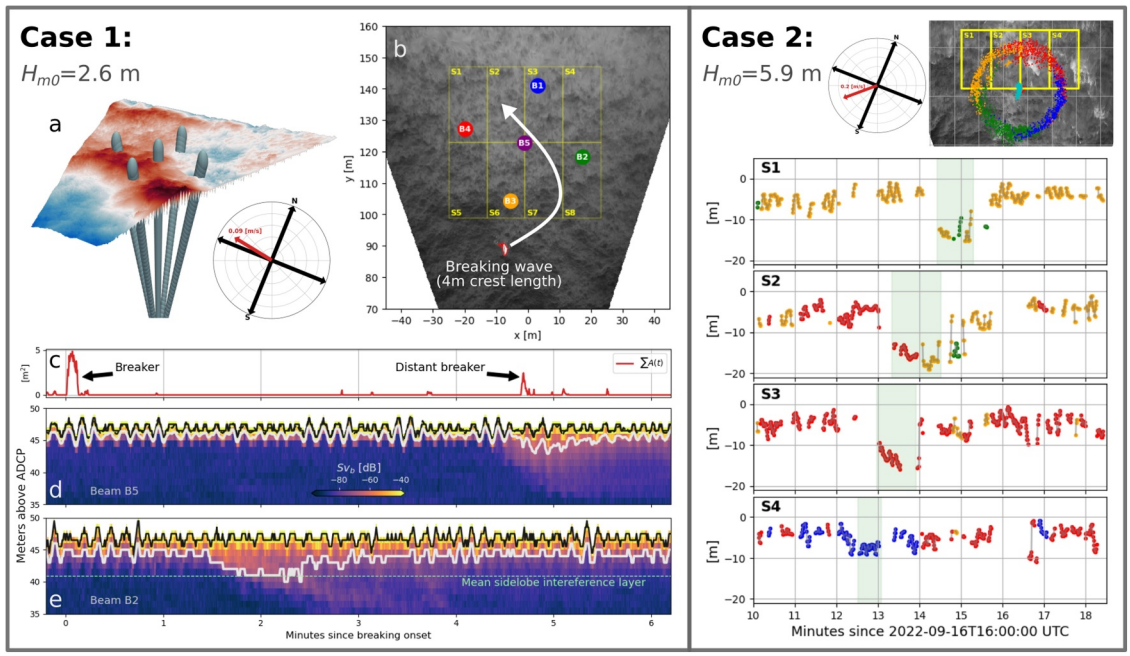

Figure 3. Demonstrating the non-local appearance of deep bubble plumes, by combining surface whitecap detection from AWDAT and the full five-beam configuration of the ADCP. Case 1 panel (a) shows a geo-referenced view of the combined observation geometry of the ADCP and the reconstructed surface from the stereo video system; panel (b) shows an ortho-rectified projection where the arrow indicate the hypothesized plume trajectory. The compass belongs to the latter view and shows the mean current. Panels (c–e) show time series of the whitecap area, burst-mode (low resolution) volumetric backscatter from beam B5, and burst-mode backscatter from beam B2, respectively. White lines in the two latter panels indicate the penetration depth of $z_{b,1}$. Case 2 shows the temporal advection of a bubble plume across segments S1–S4 in a more energetic sea state. Here, the y-axis indicates the vertical coordinate following the sea surface and the colors indicate beams 1–4 (see panel b, Case 1).

the rotation of the ADCP (up to 90° over a peak wave period), the different beams yielded redundant detections of the plume in each of the segments. This adds confidence to the interpretation that the observed feature represents the same plume and is not an artifact of an individual observation. The horizontal advection of the plume matches the direction (westward) and magnitude (0.2 m s^{-1}) of the current, corresponding to a distance of 35 m in about 3 min. Note that the plume depth is much larger than the sidelobe interference layer (about 5 m, see Supporting Information S1).

6. Discussion

6.1. Whitecaps and Bubble Depths

Using collocated measurements from stereo video and ADCP, we were able to measure both the whitecap area from above and the bubble depths from below the sea surface (Figure 1). Our data confirmed a relationship between the surface whitecaps in the vicinity of the ADCP and the high-threshold bubble detection method (BDM2) (Figures 1 and 2). This increase in backscatter intensity likely represents both large bubbles entrained by active breaking, but also a higher void fraction of smaller bubbles (Derakhti et al., 2024). We found no direct spatial or temporal connection between surface whitecaps and the single-point bubble penetration depths inferred from the low-threshold method (BDM1). Thus, the active near-surface layer of the BDM2 estimates is locally connected to the surface whitecap events, while the deeper layer of the BDM1 estimates represents entrained bubbles from non-local breakers.

By extending the $z_{b,1}$ detection to the four slanted ADCP beams, we obtain a spatially comprehensive view of the bubble plume dynamics (Figure 3). The evidence of horizontal plume advection is consistent with the hypothesis raised by Czerski et al. (2022), that there exists a deep bubble plume layer that is dynamically different from the shallow subsurface layer. Based on these results, we argue that the poor fit between whitecap coverage and mean bubble depths reported by Cifuentes-Lorenzen et al. (2023) is due to the detection of small bubbles (the study used backscatter thresholds between −60 and −70 dB), which follow dynamics that are seemingly disconnected from the whitecaps.

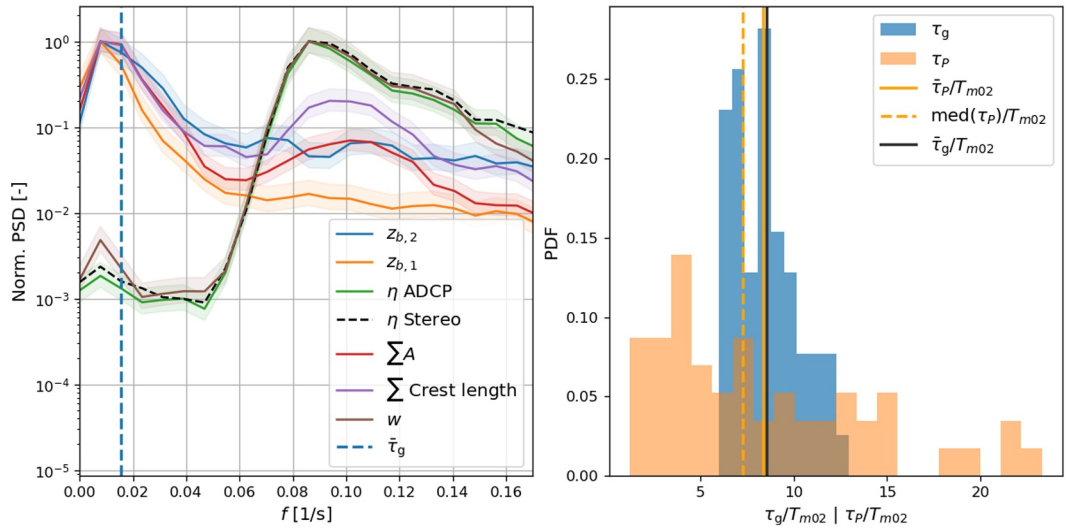

Figure 4. Left panel: Normalized power spectral density (PSD) plots for relevant sea state quantities derived from WASS/AWDAT (η, ΣA, and ΣCrest length) and the ADCP ($z_{b,1}, z_{b,2}, \eta, w, \bar{\tau}_g$), for all data acquired by each instrument within a 3-hr period (16-09-2022 15–18 UTC). Color shaded regions represent the 95% confidence interval. Right panel: The probability density function of normalized wave group (τ_g) and bubble plume time scales (τ_P) for the 3 hr period. Vertical lines denote the mean (overbar) and median (med) values. Note that med(τ_g) $\simeq \bar{\tau}_g$ and is therefore not plotted.

6.2. A Spectral View of Whitecaps and Bubble Depths

The normalized spectral response of the bubble depths, sea surface elevation, whitecap area and crest length, and the vertical velocities (from beam B5) are shown for all available data during the 3-hr period between T15–T18 at 2022–09 in Figure 4 (i.e., 60 min of ADCP data and 80 min of stereo-video data). The sea state can be considered weakly stationary for this period (Figure S3 in Supporting Information S1), and the spectral processing parameters is elaborated upon in Section S7 of Supporting Information S1.

The spectra suggest a modulation of bubble depths and wave breaking at time scales similar to the mean wave group period $\bar{\tau}_g$ (Table 1). Both the sum of whitecap area and breaking crest length have bi-modal spectra, with peaks on the group time scales and around the peak period. These time scales can be explained by two mechanisms. First, the most intense wave breaking occurs close to center of the wave groups (Figure 2, see also Malila et al. (2022)). Second, the smaller waves break at the crest of the longer, more energetic, waves around the peak frequency. However, the mean wave plume periods $\overline{\tau_P}$ appear on similar time scales as the wave groups, but the plumes themselves are out of phase with the wave groups (Figure 2).

Furthermore, the data confirm the presence of a slowly oscillating vertical velocity w (vertically averaged between 5 and 20 m), occurring at time scales longer than the wave groups. This slow mode supports the idea of Langmuir-type circulation that vertically advects small bubbles in the water column, which is in line with the observations by Fisher and Nidzieko (2024) and Scully and Zippel (2024).

Non-zero crossing variables like ΣA, ΣCrest length and $z_{b,(1,2)}$ may not be ideal for Fourier analysis. The right panel of Figure 4 therefore shows the probability density function for the group and plume time scales from a threshold-crossing analysis with respect to their definition, denoted by τ_g and τ_P, respectively. As expected, the spread in plume period is much larger than the group period, since some plumes are long lived features which are advected by the ambient currents (see Case 1, Figure 3). With our definition of bubble plumes and wave groups (Sections S4 and S5 in Supporting Information S1), the ratio of the respective periods $\bar{\tau}_P/\bar{\tau}_g = 0.98$, which indicates that there is a connection between the whitecaps and bubble plumes on the wave group time scales. However, our limited-size data set cannot be used to draw any definitive conclusions on this topic.

7. Conclusions

We have investigated open-ocean field measurements of surface whitecaps and sub-surface bubbles retrieved from a stereo video system and an ADCP, respectively. By comparing the whitecaps and bubble depth estimates —including a spatially comprehensive view of the bubble plume dynamics—we conclude that

- High-threshold bubble detection method (BDM2) represents the entrainment of bubbles in a shallow near-surface layer, which is directly connected to the surface whitecap activity
- Low-threshold bubble detection method (BDM1) represents a deeper wave-induced mixing layer, where the locally measured depths are disconnected from the local breakers, and where the main drivers are likely small-scale wave-induced currents superimposed on the mean background currents.

More measurements are needed to draw firmer conclusions on this topic. In particular, a broader range of sea states should be sampled, using instruments capable of measuring the bubble size distribution and small-scale currents.

Conflict of Interest

The authors declare no conflicts of interest relevant to this study.

Data Availability Statement

The raw and processed data used producing the figures within this manuscript is publicly available in a repository release via Halsne and Bjørnestad (2025).

Acknowledgments

We are indebted to Lars Bahr at ConocoPhillips Norway the crew onboard the OneSubSea Skandi Hugen for the help in acquiring the data. MB and ØB gratefully acknowledge the support by the Research Council of Norway through the ENTIRE project (Grant 324227). TH would like to thank Torstein Pedersen and colleagues at NORTEK A/S for fruitful discussions, and Yaron Toledo and Johannes Gemmrich for interesting discussions. MP was supported by DAIS-Ca' Foscari University through the IRIDE Program. AHC would like to acknowledge funding from the UK Natural Environment Research Council [Grant NE/T000309/1]. JP was supported by a PhD Scholarship from the NERC-funded Science and Solutions for a Changing Planet Doctoral Training Partnership administered by the Grantham Institute at Imperial College London.

References

Andriatis, A., Lenain, L., Alford, M. H., Winstead, N., & Geiman, J. (2024). Observations and numerical simulations of the onset and growth of Langmuir circulations. *Journal of Physical Oceanography*, *54*(8), 1737–1763. https://doi.org/10.1175/JPO-D-24-0004.1

Benetazzo, A., Fedele, F., Gallego, G., Shih, P.-C., & Yezzi, A. (2012). Offshore stereo measurements of gravity waves. *Coastal Engineering*, *64*, 127–138. https://doi.org/10.1016/j.coastaleng.2012.01.007

Benetazzo, A., Halsne, T., Breivik, Ø., Strand, K. O., Callaghan, A. H., Barbariol, F., et al. (2024). On the short-term response of entrained air bubbles in the upper ocean: A case study in the north Adriatic Sea. *Ocean Science*, *20*(3), 639–660. https://doi.org/10.5194/os-20-639-2024

Benetazzo, A., Halsne, T., Breivik, Ø., Strand, K. O., Callaghan, A., Barbariol, F., et al. (2023). On the short-term response of entrained air bubbles in the upper ocean: A case study in the North Adriatic Sea. *EGUsphere*, 1–32. https://doi.org/10.5194/egusphere-2023-2387

Bergamasco, F., Torsello, A., Sclavo, M., Barbariol, F., & Benetazzo, A. (2017). WASS: An open-source pipeline for 3D stereo reconstruction of ocean waves. *Computers & Geosciences*, *107*, 28–36. https://doi.org/10.1016/j.cageo.2017.07.001

Breivik, Ø., Carrasco, A., Haakenstad, H., Aarnes, O. J., Behrens, A., Bidlot, J.-R., et al. (2022). The impact of a reduced high-wind Charnock coefficient on wave growth with application to the North Sea, the Norwegian Sea and the Arctic Ocean. *Journal of Geophysical Research: Oceans*, *127*(3), e2021JC018196. https://doi.org/10.1029/2021JC018196

Callaghan, A., Deane, G., & Stokes, M. (2016). Laboratory air-entraining breaking waves: Imaging visible foam signatures to estimate energy dissipation. *Geophysical Research Letters*, *43*(21), 11–320. https://doi.org/10.1002/2016GL071226

Callaghan, A., Deane, G., & Stokes, M. (2017). On the imprint of surfactant-driven stabilization of laboratory breaking wave foam with comparison to oceanic whitecaps. *Journal of Geophysical Research: Oceans*, *122*(8), 6110–6128. https://doi.org/10.1002/2017jc012809

Callaghan, A., Deane, G., & Stokes, M. D. (2024). A comparison of laboratory and field measurements of whitecap foam evolution from breaking waves. *Journal of Geophysical Research: Oceans*, *129*(1), e2023JC020193. https://doi.org/10.1029/2023JC020193

Cifuentes-Lorenzen, A., Zappa, C. J., Randolph, K., & Edson, J. B. (2023). Scaling the bubble penetration depth in the ocean. *Journal of Geophysical Research: Oceans*, *128*(9), e2022JC019582. https://doi.org/10.1029/2022JC019582

Czerski, H., Brooks, I. M., Gunn, S., Pascal, R., Matei, A., & Blomquist, B. (2022). Ocean bubbles under high wind conditions – Part 1: Bubble distribution and development. *Ocean Science*, *18*(3), 565–586. (Publisher: Copernicus GmbH). https://doi.org/10.5194/os-18-565-2022

Deane, G. B., & Stokes, M. D. (2010). Model calculations of the underwater noise of breaking waves and comparison with experiment. *Journal of the Acoustical Society of America*, *127*(6), 3394–3410. https://doi.org/10.1121/1.3419774

Deike, L. (2022). Mass transfer at the ocean–atmosphere interface: The role of wave breaking, droplets, and bubbles. *Annual Review of Fluid Mechanics*, *54*(1), 191–224. https://doi.org/10.1146/annurev-fluid-030121-014132

Deike, L., Pizzo, N., & Melville, W. K. (2017). Lagrangian transport by breaking surface waves. *Journal of Fluid Mechanics*, *829*, 364–391. https://doi.org/10.1017/jfm.2017.548

Derakhti, M., Thomson, J., Bassett, C., Malila, M., & Kirby, J. T. (2024). Statistics of bubble plumes generated by breaking surface waves. *Journal of Geophysical Research: Oceans*, *129*(5), e2023JC019753. https://doi.org/10.1029/2023JC019753

Farmer, D., McNeil, C., & Johnson, B. (1993). Evidence for the importance of bubbles in increasing air–sea gas flux. *Nature*, *361*(6413), 620–623. https://doi.org/10.1038/361620a0

Farmer, D. M., Vagle, S., & Booth, A. D. (1998). A free-flooding acoustical resonator for measurement of bubble size distributions. *Journal of Atmospheric and Oceanic Technology*, *15*(5), 1132–1146. https://doi.org/10.1175/1520-0426(1998)015⟨1132:AFFARF⟩2.0.CO;2

Fisher, A. W., & Nidzieko, N. J. (2024). Auv observations of Langmuir turbulence in a stratified shelf sea. *Journal of Physical Oceanography*, *54*(9), 1903–1920. https://doi.org/10.1175/jpo-d-23-0136.1

Haakenstad, H., Breivik, Ø., Furevik, B. R., Reistad, M., Bohlinger, P., & Aarnes, O. J. (2021). NORA3: A nonhydrostatic high-resolution hindcast of the north sea, the Norwegian Sea, and the Barents Sea. *Journal of Applied Meteorology and Climatology*, *60*(10), 1443–1464. https://doi.org/10.1175/JAMC-D-21-0029.1

Halsne, T., & Bjørnestad, M. (2025). Source codes and data for the Ekofisk 2022 campaign. *GitHub*. https://doi.org/10.5281/zenodo.15690116
Leibovich, S. (1983). The form and dynamics of Langmuir circulations. *Annual Review of Fluid Mechanics*, *15*(1), 391–427. https://doi.org/10.1146/annurev.fl.15.010183.002135
Liang, J.-H., McWilliams, J. C., Sullivan, P. P., & Baschek, B. (2012). Large eddy simulation of the bubbly ocean: New insights on subsurface bubble distribution and bubble-mediated gas transfer. *Journal of Geophysical Research*, *117*(C4). https://doi.org/10.1029/2011jc007766
Longuet-Higgins, M. S. (1984). Statistical properties of wave groups in a random sea state. *Philosophical Transactions of the Royal Society of London—Series A: Mathematical and Physical Sciences*, *312*(1521), 219–250. https://doi.org/10.1098/rsta.1984.0061
Malila, M. P., Thomson, J., Breivik, Ø., Benetazzo, A., Scanlon, B., & Ward, B. (2022). On the groupiness and intermittency of oceanic whitecaps. *Journal of Geophysical Research: Oceans*, *127*(1), e2021JC017938. https://doi.org/10.1029/2021JC017938
McWilliams, J. C., Sullivan, P. P., & Moeng, C.-H. (1997). Langmuir turbulence in the ocean. *Journal of Fluid Mechanics*, *334*, 1–30. https://doi.org/10.1017/S0022112096004375
Peach, J., Callaghan, A. H., Bergamasco, F., Pistellato, M., Barbariol, F., & Benetazzo, A. (2025). A vision-based method for spatial and temporal tracking of individual whitecaps from breaking ocean waves. *IEEE Transactions on Geoscience and Remote Sensing*, *63*, 1–15. https://doi.org/10.1109/TGRS.2025.3555851
Peláez-Zapata, D., Pakrashi, V., & Dias, F. (2024). Dynamics of bubble plumes produced by breaking waves. *Journal of Physical Oceanography*. https://doi.org/10.1175/JPO-D-23-0261.1
Pistellato, M., Bergamasco, F., Torsello, A., Barbariol, F., Yoo, J., Jeong, J.-Y., & Benetazzo, A. (2021). A physics-driven CNN model for real-time sea waves 3d reconstruction. *Remote Sensing*, *13*(18), 3780. https://doi.org/10.3390/rs13183780
Pizzo, N. E., Deike, L., & Melville, W. K. (2016). Current generation by deep-water breaking waves. *Journal of Fluid Mechanics*, *803*, 275–291. https://doi.org/10.1017/jfm.2016.469
Pizzo, N. E., & Melville, W. K. (2013). Vortex generation by deep-water breaking waves. *Journal of Fluid Mechanics*, *734*, 198–218. https://doi.org/10.1017/jfm.2013.453
Scully, M. E., & Zippel, S. F. (2024). Vertical energy fluxes driven by the interaction between wave groups and Langmuir turbulence. *Journal of Physical Oceanography*, *54*(7), 1347–1366. https://doi.org/10.1175/JPO-D-23-0193.1
Strand, K. O., Breivik, Ø., Pedersen, G., Vikebø, F. B., Sundby, S., & Christensen, K. H. (2020). Long-term statistics of observed bubble depth versus modeled wave dissipation. *Journal of Geophysical Research: Oceans*, *125*(2), e2019JC015906. https://doi.org/10.1029/2019JC015906
Thorpe, S., Osborn, T., Farmer, D., & Vagle, S. (2003). Bubble clouds and Langmuir circulation: Observations and models. *Journal of Physical Oceanography*, *33*(9), 2013–2031. https://doi.org/10.1175/1520-0485(2003)033<2013:bcalco>2.0.co;2
Thorpe, S. A. (1982). On the clouds of bubbles formed by breaking wind-waves in deep water, and their role in air-sea gas transfer. *Philosophical Transactions of the Royal Society of London—Series A: Mathematical and Physical Sciences*, *304*(1483), 155–210. (Publisher: Royal Society). https://doi.org/10.1098/rsta.1982.0011
Thorpe, S. A. (1984). On the determination of Kv in the near-surface ocean from Acoustic measurements of Bubbles.
Vagle, S., & Farmer, D. (1998). A comparison of four methods for bubble size and void fraction measurements. *IEEE Journal of Oceanic Engineering*, *23*(3), 211–222. https://doi.org/10.1109/48.701193
Vagle, S., & Farmer, D. M. (1992). The measurement of bubble-size distributions by acoustical backscatter. *Journal of Atmospheric and Oceanic Technology*, *9*(5), 630–644. https://doi.org/10.1175/1520-0426(1992)009⟨0630:TMOBSD⟩2.0.CO;2
Vagle, S., McNeil, C., & Steiner, N. (2010). Upper ocean bubble measurements from the NE Pacific and estimates of their role in air-sea gas transfer of the weakly soluble gases nitrogen and oxygen. *Journal of Geophysical Research*, *115*(C12). https://doi.org/10.1029/2009JC005990
Woolf, D. K. (1997). Bubbles and their role in gas exchange. In *The sea surface and global change* (pp. 173–206). Cambridge University Press.

Erratum

Since the original publication of this article the affiliation of coauthor Joe Peach has been changed to Department of Civil and Environmental Engineering, Imperial College London, South Kensington, UK. The affiliation of coauthor Göran Broström has been changed to Norwegian Meteorological Institute, Bergen, Norway and Department of Earth Science, University of Gothenburg, Gothenburg, Sweden. This may be considered the authoritative version of record.